

UDC 544.723

COMPARATIVE ANALYSIS OF POROUS STRUCTURE AND ADSORPTION PROPERTIES OF ACTIVATED CARBONS

V.M. Gun'ko^{1*}, R. Leboda², J. Skubiszewska-Zięba², V.I. Zarko¹,
E.V. Goncharuk¹, B. Charmas², S.V. Mikhalkovsky³

¹ Chuiko Institute of Surface Chemistry of National Academy of Sciences of Ukraine
17 General Naumov Str., Kiev, 03164, Ukraine

² Maria Curie-Skłodowska University, Faculty of Chemistry

³ Maria Curie-Skłodowska pl., Lublin, 20031, Poland

³ University of Brighton, School of Pharmacy & Biomolecular Sciences
Brighton, BN2 4GJ, United Kingdom

Analysis of porous structure of a variety of activated carbons, ACs, produced from natural raw materials or polymers has been carried out using SEM, AFM, TEM, adsorption, DSC and TG/DTA methods. Despite great porosity and high specific surface area, ACs poorly adsorb water from air. However, larger amounts of water fill a major portion (but incompletely) of the pore volume of ACs immersed in liquid water or wetted by liquid water but the heat of immersion in water is much smaller than that for decane. The pore size distributions (PSD) calculated from the adsorption and DSC data are in agreement with the PSD based on the analysis of HRTEM images.

INTRODUCTION

Structural features of activated carbons and related materials have been analysed in detail by many authors [1–14]. However, new experimental or calculations methods can stimulate deeper insight into the problem of adequate structural characterisation of ACs. For instance, the appearance of different versions of density functional theory (DFT) [15–20], progress in Monte-Carlo simulations of carbons [21–25] as well as high-resolution transmission electron microscopy (HRTEM), scanning electron microscopy (SEM), small angle X-ray scattering (SAXS) and other methods applied to different ACs stimulated new investigations of structural features of a variety of the materials [5, 14].

It should be noted that IUPAC recommended term ‘micropores’ is rather incompatible with term ‘nanoparticles’ (which can possess ‘micropores’) since ‘micro’ corresponds to 10^{-6} but ‘nano’ is 10^{-9} . In other words, smaller scale nano ($\sim 10^{-9}$) particles include larger scale micro (10^{-6}) pores; however, pore sizes should be really smaller than particle sizes. Therefore, in this paper, obsolete term ‘micropores’ (recommended by IUPAC) corresponding to pores with half-width $x < 1$ nm has been replaced by term ‘nanopores’.

According to HRTEM and SEM images [14], the pore structure of ACs is more complex than that of highly oriented graphitic materials comprising stacks of ideal or nearly ideal flat carbon sheets with narrow slit-shaped pores (nanopores) between them. Therefore, modern gas adsorption instruments include firm software with DFT methods with complex models of pores for carbons, e.g. slit-shaped/cylindrical pores [26]. Monte Carlo models developed for ACs [14, 21–25] and HRTEM images of carbons [14, 27–32] suggest that there are significant deviations in the AC pore structure from a simple model of slit-shaped pores between planar carbon sheets because these sheets can be non-planar, especially for mesopores ($1 < x < 25$ nm) and macropores ($x > 25$ nm).

HRTEM can give useful information on the structure of nanoporous nanoparticles (NPNP) [14, 27–32]. However, frequently these images have been used to obtain only qualitative information which could be difficult to be compared with the pore size distributions (PSDs) based on the adsorption methods or other quantitative characteristics of carbons. Some authors used HRTEM to obtain the PSDs of nanopores [31] using two-dimensional fast Fourier transform (FFT) that can result in the PSDs with certain errors. As a whole, the problem of quantitative comparison of

* corresponding author vlad_gunko@ukr.net
ХФТП 2012. Т. 3. № 2

the PSDs based on the adsorption (with respect to very narrow nanopores) and HRTEM (with respect to accurate quantitative analysis of images of pores in the nanoscale range) methods needs additional investigations. Therefore, the aim of this paper is to compare the PSDs of a carbonisate (of a phenol formaldehyde resin precursor) and the corresponding AC (50 % burn-off degree) based on the nitrogen adsorption data (treated using several methods: DFT, NLDFT, QSDFT, MND) and quantitative analysis of HRTEM images (using ImageJ and Fiji software developed for direct qualitative analysis of images), as well as the burn-off degree effects on the PSDs of nanopores, DSC and TG/DTA data for a set of AC samples.

EXPERIMENTAL

Materials

Several sets of ACs were analysed here: (i) two series of ACs produced from plum stones (PSO MASKPOL and HPSD, Hajnowka, Poland) [33–38], (ii) ACs from coconut shells (A.U.G. Aktivekohle, Germany) [33], (iii) AC Norit R 0.8 Extra (Norit NV, The Netherlands; granules have a regular cylindrical form at $d = 0.8$ mm) [39], (iv) porous phenol formaldehyde resin beads carbonised by heating in a CO_2 flow to 1073 K at a ramp of 3 K/min (sample labelled as C-0), then sieving samples of 250–500 μm in size have been additionally activated in CO_2 flow at 1183 K with different residence times producing ACs with different burn-off degree 25–86 % (MAST Carbon International Ltd, UK) [40–45]; (v) ACs prepared with the C-0 sample as initial one activated by water vapour in a fixed bed reactor, similar to activation by CO_2 (labelled Wf- x , $x = 24$ –77 % burn-off degree) and in a fluidised bed reactor at 1020–1050 K (labelled W- x , $x = 42.5$ –88.3 % burn-off degree at bulk density of 0.18–0.10 g/cm^3 , respectively) [44].

Methods

The textural characteristics of ACs calculated with the DFT (slit-shaped, S, and slit-shaped-cylindrical (SC) pore models) and MND (SC pores and voids between nanoparticles, SCV-model, with a self-consistent regularisation procedure, SCR) are shown in Table 1.

The structural characteristics of carbonisates and AC samples have been determined from the nitrogen adsorption-desorption isotherms recorded at 77.4 K using a Micromeritics ASAP 2010 (or 2405N) adsorption analyser or a Quantachrome Autosorb adsorption analyser. The pore size

distributions (differential $\sim dV/dx$) have been calculated with the quenched solid density functional theory (QSDFT) method with the S-model and nonlocal DFT (NLDFT) with the SC-model (Quantachrome software, version 2.02) [26]. Additionally, to show a complex pore shape of activated carbons, the SC-model with voids between nanoparticles (SCV-model) with the SCR procedure was applied [46] with the modified Nguyen-Do [47] (MND) method [46]. The DFT method [48] with the S-model was also used. The SCV/SCR method allows us to estimate the contributions of different types of pores into the total porosity. The differential PSD functions with respect to the pore volume ($\text{PSD}_V, f_V(x) \sim dV/dx, \int f_V(x)dx \sim V_p$) and the specific surface area ($\text{PSD}_S, f_S(x) \sim dS/dx, \int f_S(x)dx \sim S$) were applied to estimate the contribution of nano- ($x < 1$ nm), meso- ($1 < x < 25$ nm) and macropores ($x > 25$ nm), as well as the deviation (Δw) of the pore shape from the S- or SCV-models of pores [49] (Table 1).

HRTEM images have been obtained with a JEOL 2010FX TEM apparatus operated at 200 kV (at Centre for Advanced Microscopy, University of Reading, UK) [27, 28]. HRTEM images have been analysed using the Fiji (local thickness plugin) [50] and ImageJ (granulometry plugin) [51] software to calculate the PSDs of nanopores [52].

Scanning electron microscopy (SEM) images were recorded using a Tesla BS-301 (Tesla, Czech Republic) SEM apparatus.

Atomic Force Microscopic (AFM) images of a set of ACs were obtained by means of a NanoScope III (Digital Instruments, USA) apparatus using a tapping mode AFM measurement technique.

A study of a set of AC samples was carried out by means of a DAC 1.1A (EPSE, Chernogolovka, Russia) differential automatic calorimeter. Before measurements of the heat of immersion (ΔH_{im}) in water or decane, a sample (~50 mg) was degassed at 393 K and 0.01 Pa for 2 h. Used amount of sample was 50 mg per 3 cm^3 of distilled water or decane exposed for several hours. The average errors of the ΔH_{im} measurements repeated several times were smaller than ± 10 %. Differential scanning calorimetry (DSC) measurements were carried out with a PerkinElmer DSC apparatus.

Water or other liquids can be frozen in narrower pores at lower temperatures that can be described by the Gibbs-Thomson relation for the freezing point

depression for liquids located in cylindrical pore of radius R_p [53, 54]

$$R_p(\text{nm}) = 0.68 - \frac{32.33}{T_m - T_{m0}}, \quad (1)$$

where T_m and T_{m0} are the melting temperatures of confined and bulk water, respectively. The pore size distribution, dV/dR can be calculated from the water melting thermograms [53, 54]

$$\frac{dV}{dR}(\text{cm}^3 \text{nm}^{-1} \text{g}^{-1}) = \frac{\frac{dq}{dt}(T_m - T_{m0})^2}{32.33\rho\beta m\Delta H(T)}, \quad (2)$$

where dq/dt , ρ , β , m and $\Delta H(T)$ are the DSC heat flow, the water density, the heating rate, the sample mass and the melting enthalpy of water, respectively. The ΔH value as a function of temperature can be estimated as follows [54]

$$\Delta H(T)(\text{J g}^{-1}) = 332 + 11.39(T_m - T_{m0}) + 0.155(T_m - T_{m0})^2. \quad (3)$$

Thermogravimetry (TG) with differential thermal analysis (DTA) of ACs was carried out in air at 293–573 or 293–1273 K using a Q apparatus (Derivatograph-C, Paulik, Paulik & Erdey, MOM, Budapest) at a heating rate of 10 K/min. Typically water adsorption (< 10 wt. %) on samples before TG measurement occurred in air, but certain samples were in a dessicator with saturated water vapour for 72 h that resulted in 50–60 wt. % adsorption of water. This difference in the water adsorption by ACs studied is due to textural features of carbons (nano/meso/macroporous), a relatively low content of O-containing functionalities, and low partial pressure of water in air [34–49].

Table 1. Textural characteristics of carbonisates and activated carbons

AC	S_{BET} , m^2/g	S_{nano} , m^2/g	S_{meso} , m^2/g	S_{macro} , m^2/g	V_p , cm^3/g	V_{nano} , cm^3/g	V_{meso} , cm^3/g	V_{macro} , cm^3/g	Δw
C-0	590	550	33	7	0.950	0.326	0.235	0.389	-0.171 ^c
C-50	1664	1460	84	10	1.486	0.745	0.328	0.413	0.143 ^c
C-0*	534	498	28	8	0.902	0.284	0.188	0.430	-0.169 ^c
C-29	1042	991	43	8	1.310	0.542	0.241	0.527	-0.111 ^c
C-47	1433	1348	73	11	1.675	0.720	0.351	0.604	-0.057 ^c
C-65	2019	1872	134	13	1.857	0.812	0.543	0.502	0.261 ^c
C-0**	549	493	45	11	0.981	0.259	0.253	0.469	0.007
C-25	1082	1011	65	6	1.011	0.511	0.314	0.187	0.061
C-45	1615	1510	101	4	1.319	0.751	0.406	0.162	0.132
C-62	2270	2090	175	4	1.683	1.004	0.505	0.175	0.240
C-75	3047	2626	413	6	2.349	1.223	0.904	0.222	0.334
C-86	3463	2181	1279	3	2.320	1.314	0.887	0.119	0.304
C-86 ^b	3463	1490	1969	4	2.320	0.606	1.567	0.148	0.626
C-30 ^a	1145	1052	88	5	1.187	0.554	0.469	0.164	0.157
C-60	1999	1729	250	19	1.969	0.663	0.638	0.669	0.561
Wf-24	963	894	67	3	0.908	0.460	0.352	0.095	0.084
Wf-45	1194	1199	91	5	1.208	0.620	0.427	0.162	0.098
Wf-66	1780	1606	171	5	1.606	0.806	0.627	0.173	0.206
Wf-77	2080	1826	253	3	1.826	0.894	0.563	0.122	0.268
W-43	1189	1118	62	9	1.235	0.579	0.270	0.386	0.157
W-59	1677	1553	118	5	1.442	0.785	0.446	0.211	0.222
W-73	2069	1855	208	6	1.825	0.918	0.671	0.236	0.265
W-88	2793	2288	500	6	2.350	1.105	1.105	0.230	0.329
W-88 ^b	2793	786	1989	19	2.350	0.544	1.458	0.348	0.588

Note. C-0, C-0* and C-0** are different carbonisates prepared with the same precursor. Contribution of nanopores (S_{nano} , V_{nano}) at half-width $x < 1$ nm, mesopores (S_{meso} , V_{meso}) at $1 < x < 25$ nm, and macropores (S_{macro} , V_{macro}) at $x > 25$ nm; Δw is the relative deviation of the pore shape from the slitshaped or ^cslitshaped-cylindrical models. ^aC-30 was catalytically activated. ^bModel with a mixture of slitshaped (relative contribution 0.533 and 0.534 for C-86 and W-88, respectively) and cylindrical (0.335 and 0.363) pores and voids between spherical nanoparticles (0.132 and 0.103) was used with the SCR procedure.

Results and discussion

Typically spherical AC particles have a certain, frequently narrow distribution in size (Fig. 1). All the AC samples studied have particle sizes between 1 and 500 μm [33–45]. Therefore, the external surface area of carbon particles is not higher than several m^2/g . The surface of particles is not smooth (Figs. 1 and 2) that can slightly add the external surface area, which however remains much smaller than the internal specific surface area, e.g. superactivated ACs have $S_{\text{BET}} = 2000\text{--}3500 \text{ m}^2/\text{g}$ (Table 1). Consequently, the adsorption properties of ACs are mainly determined by the inner texture of AC nanoparticles (with nanopores, i.e. NPNP) and their aggregates (voids between NPNPs correspond to meso- and macropores). ACs can be divided into pure nanoporous (I), nano/mesoporous (II), and nano/meso/macroporous (III) ACs.

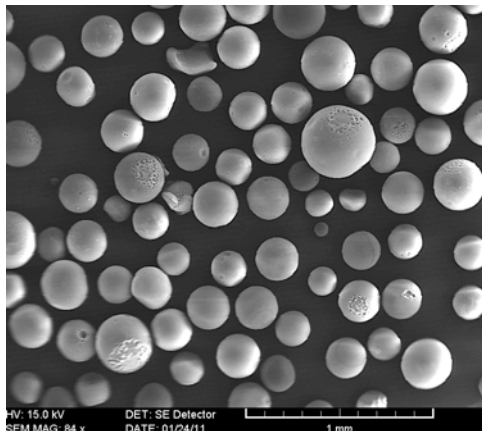


Fig. 1. SEM image of activated carbons C-65

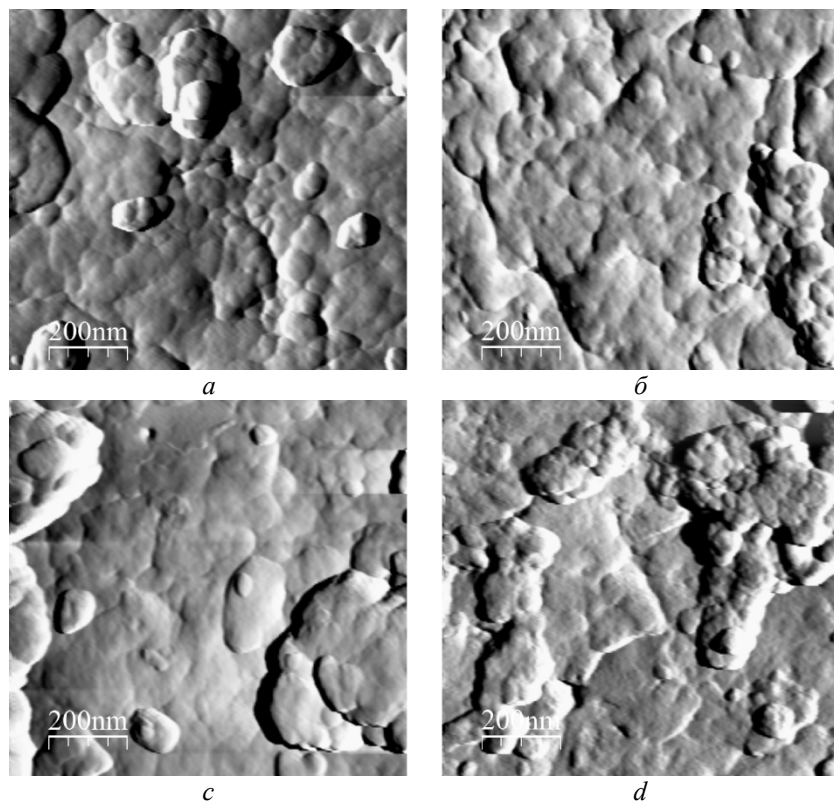


Fig. 2. AFM images of activated carbons: C-0 (a), C-29 (b), C-47 (c) and C-65 (d)

For each AC group, the nitrogen adsorption isotherms have certain features. For instance, ACs I have the isotherms which reach the plateau adsorption at low pressures $p/p_0 < 0.1$ (Fig. 3). For ACs II, a certain increase in the adsorption is observed at $p/p_0 > 0.1$; however,

there is no strong increase in the adsorption at $p/p_0 > 0.8$. If this increase is observed, ACs correspond to the materials of the group III (Fig. 3, Table 1). Some of ACs III have a larger contribution of macropores into the pore volume than mesopores (Fig. 4, Table 1).

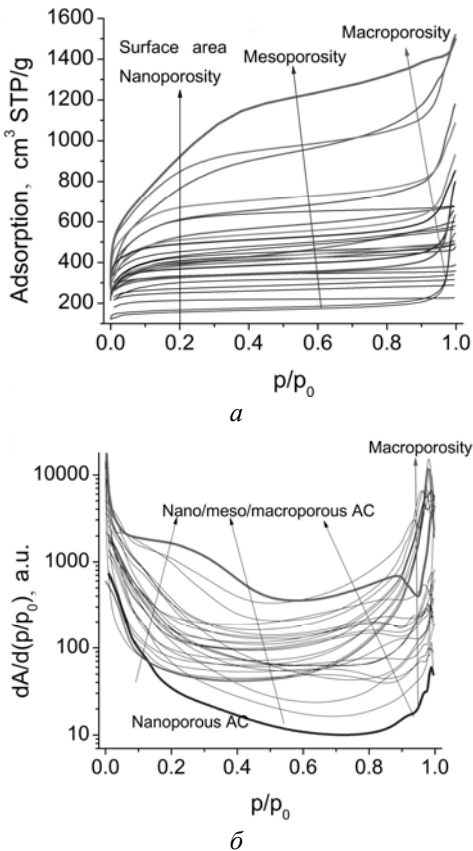


Fig. 3. Nitrogen adsorption isotherms (*a*) and corresponding derivatives for 28 samples of carbonisates and activated carbons at the S_{BET} value from 500 to $3463 \text{ m}^2/\text{g}$ (*b*)

The derivatives of the nitrogen adsorption isotherms (Fig. 3, *b*) as well as the PSDs (Figs. 4 and 5) show that contribution of middle mesopores at $2 < x < 10 \text{ nm}$ is relatively low. This structural feature is caused by the origin of pores over different ranges. Nanopores ($x < 1 \text{ nm}$) and narrow mesopores ($1 < x < 2-3 \text{ nm}$) are inner pores in nanoparticles (NPNPs) of 20–40 nm in size [52]. Middle mesopores are absent in these NPNPs due to their sizes in the same range corresponding to the mentioned mesopores. Larger mesopores and macropores correspond to voids between the NPNPs in their aggregates. Large macropores are voids between the aggregates forming AC granules (Fig. 1).

The main advantages of ACs as adsorbents are linked to a large number of nanopores in NPNPs with a high adsorption potential for molecules and ions of non-polymeric compounds. Therefore, the exact characterisation of nanopores is of importance from both practical and theoretical points of view. HRTEM gives a detailed picture of nanopores but this picture *per se* gives only qualitative information.

To obtain quantitative information from HRTEM images, special software should be used [52]. Calculations of the PSDs based on HRTEM images give results similar to the QSDFT PSDs (Fig. 6). HRTEM/Fiji PSDs having a shape of narrow peaks correspond to thin stacks with removed one-three inner carbon sheets.

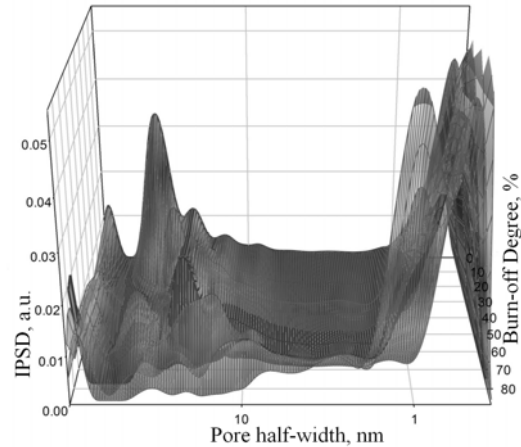


Fig. 4. Incremental PSDs (DFT, slitshaped model) for three sets of ACs activated by CO_2 and water vapour

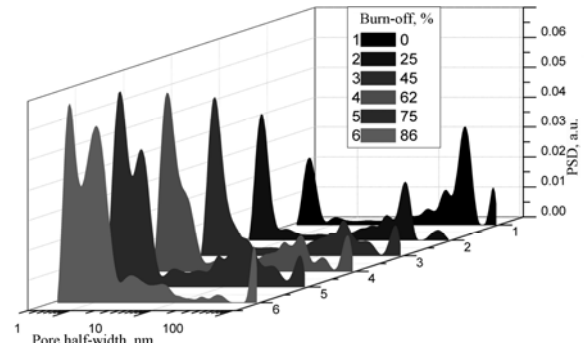


Fig. 5. IPSDs of a set of ACs activated by CO_2

It should be noted that agreement between HRTEM PSDs and NLDFT or DFT PSDs is worse than that with QSDFT PSDs because of more correct potentials of the pore walls derived in the QSDFT [20].

A complex texture of ACs and the presence of O-containing sites mainly at the edges of carbon sheets can cause a complex behaviour of adsorbed compounds, especially water [55]. The adsorption of water onto ACs from air (at low partial pressure of water vapour) occurs mainly onto hydrophilic O-containing sites (whose number is rather small). Therefore, the amounts of water adsorbed onto ACs from air at room temperature is low (< 10 wt. %) (Figs. 7 and 8) despite the large pore volume and specific surface area (Table 1). Water poorly adsorbs

in hydrophobic slit-shaped nanopores (adsorption energy is 15–20 kJ/mol [55]). Main portion of this water can be removed at $T < 373$ K. However, when ACs are being in saturated water vapour during a long period (72 h), the water adsorption strongly increases (Fig. 8). This water desorbs at higher temperatures at $T < 423$ K because it penetrates into

narrow pores and desorption from which is slower than from broad meso- and macropores. For water it is characteristic clustered adsorption therefore water tends to form large structures in large pores. However, these structures cannot be formed at low pressures before capillary condensation.

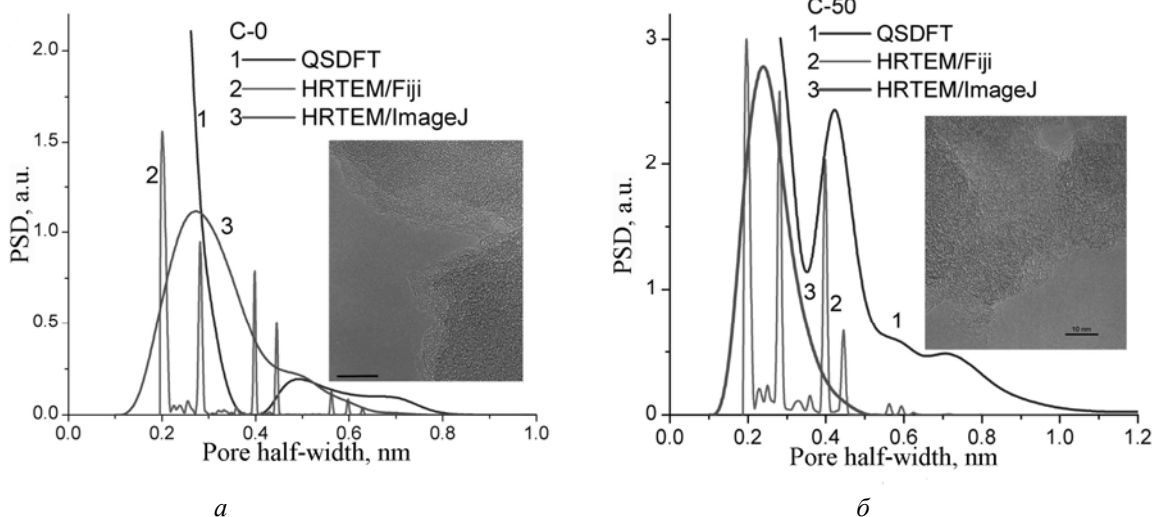


Fig. 6. Pore size distributions for carbonisate C-0 (*a*) and activated carbon C-50 (*b*) at 50 % burn-off degree from HRTEM [52] and QSDFT

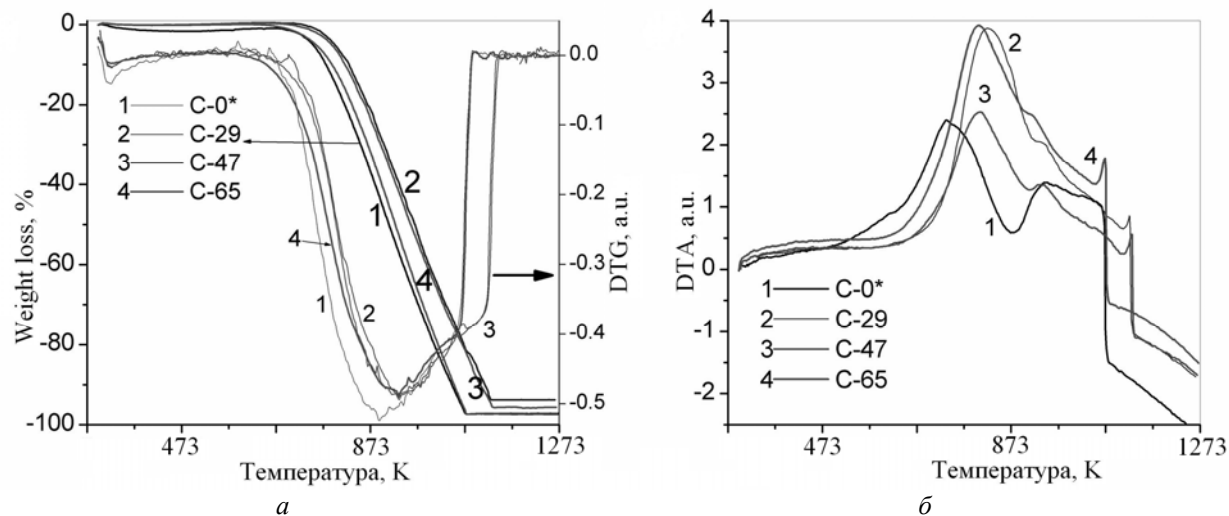


Fig. 7. TG and DTG (*a*) and DTA (*b*) curves for carbonisate C-0* and activated carbons

Adsorption/desorption of water depends relatively weakly on the specific surface area of ACs (Figs. 7 and 8) because water does not form a continuous layer but adsorbs in the form of clusters (low coverage) from air or nanodrops and nanodomains (larger coverage, capillary condensation) from saturated water vapour.

The heat of immersion of ACs in water ($\Delta H_{im,w}$) changes nonlinearly with increasing

burn-off degree (i.e. S_{BET} value) as well as $\Delta H_{im,d}$ of immersion of ACs in decane (Table 2). Therefore, the hydrophilicity of ACs estimated as the ratio $K_h = \Delta H_{im,w}/\Delta H_{im,d}$ tends to decrease with increasing burn-off degree (or S_{BET}). This result is in agreement with the TG data (Fig. 8) showing the minimal amounts of desorbed water for C-65. ACs are rather hydrophobic materials since $K_h < 1$ (Table 2). Therefore, the water

adsorption from air is low (Fig. 8) despite a large nano/mesoporosity of ACs (Table 1, Figs. 4–6).

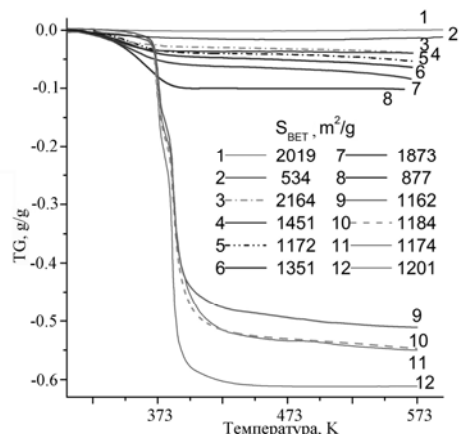


Fig. 8. TG curves for ACs various S_{BET} values; maximum water desorption ($> 0.4 \text{ g/g}$) corresponds to samples hydrated in saturated water vapour during 72 h

According to calculations with the DSC cryoporometry with Eq. (2), water added to ACs (hydration $h = 0.32\text{--}2.13 \text{ g}$ of water per gram of AC) fills only narrow pores (Fig. 9). The size of pores filled by water increases with increasing burn-off degree that is well seen for C-86. This result is due to an increase in contribution of narrow mesopores with increasing burn-off degree (Fig. 5) and a parallel decrease in the hydrophilicity of ACs (Fig. 8).

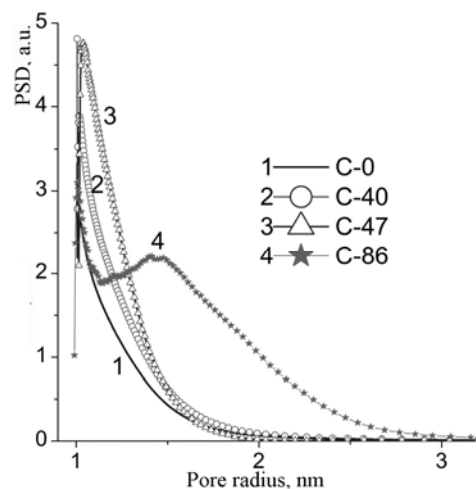


Fig. 9. Pore size distributions calculated from the DSC curves (heating of samples frozen from 293 to –374 K at a rate of 50 °/min and then heated) for hydrated carbons ($h = 0.32\text{--}2.13 \text{ g/g}$) at different burn-off degree

Table 2. Heat of immersion of carbons in water and decane and hydrophilicity coefficient

Carbon-burn-off, %	Liquid	$\Delta H_{\text{im}}, \text{J/g}$	$K_h = \Delta H_{\text{im},w}/\Delta H_{\text{im},d}$
C-0	water	24.1	
C-0	decane	73.2	
C-30	water	42.9	
C-30	decane	160.4	0.27
C-40	water	58.5	
C-40	decane	134.9	0.43
C-44	water	49.6	
C-44	decane	169.9	0.29
C-47	water	46.5	
C-47	decane	158.3	0.29

CONCLUSIONS

Practically all ACs studied have slit-shaped nanopores (pore half-width $x < 1 \text{ nm}$) and narrow mesopores ($1 < x < 2\text{--}3 \text{ nm}$) in nanoparticles. If nanoparticles are densely packed in granules, ACs do not practically have broad meso- and macropores. If this packing is less dense, the textural porosity (voids between nanoparticles in their aggregates) is observed. However, the contribution of middle mesopores ($x = 3\text{--}10 \text{ nm}$) to the total porosity is typically lower in these ACs than that of broad mesopores ($10 < x < 25 \text{ nm}$) and macropores ($x > 25 \text{ nm}$).

Despite certain hydrophobicity of ACs studied, they can adsorb great amounts of water from saturated water vapour in contrast to the adsorption from air. Water adsorbed from air forms clusters filling mainly narrow pores.

The pore size distributions calculated from HRTEM images (Fiji software), DSC data (cryoporometry), and nitrogen adsorption (QSDFT) are similar for narrow pores.

ACKNOWLEDGEMENTS

The authors are grateful to European Community, Seventh Framework Programme (FP7/2007-2013), Marie Curie International Research Staff Exchange Scheme (IRSES grant No 230790, COMPOSITUM) for financial support. The authors thank Dr. O.P. Kozynchenko (MAST Carbon International Ltd.) for sets of ACs and HRTEM images.

REFERENCES

1. Smisek M., Cerny S. Active Carbon. – Amsterdam: Elsevier, 1970. – 276 p.

2. Bansal R.C., Donnet J.B., Stoeckli F. Active Carbon. – New York: Marcel Dekker, 1988. – 482 p.
3. Gregg S.J., Sing K.S.W. Adsorption, Surface Area and Porosity. 2nd ed. San Diego: Academic Press, 1982. – 303 p.
4. McEnaney B., Mays T.J., Rodríguez-Reinoso F. Fundamental aspects of active carbons // Special issue. Carbon. – 1998. – V.36, N 10. – P. 1415–1556.
5. Marsh H., Heintz E.A., Rodríguez-Reinoso F. Introduction to Carbon Technologies: University of Alicante, 1997. – 669 p.
6. Rodríguez-Reinoso F., Linares-Solano A. Micro-porous structure of activated carbons as revealed by adsorption methods / Editor Thrower P., Chemistry and Physics of Carbon / New York: Marcell Dekker, Inc. – 1988. – V. 21. – P. 2–146.
7. Thrower P.A. The application of electron microscopy techniques to an understanding of radiation damage in graphite (Plenary Lecture) // Carbon. – 1969. – V. 7, N. 6. – P. 725.
8. Rodríguez-Reinoso F., Thrower PA, Microscopic studies of oxidized highly oriented pyrolytic graphite // Carbon 1972. – V. 10, N 3. – P. 339.
9. Thrower P.A., Jones L.E. Microscopic studies of carbon composites // Carbon. – 1984. – V. 22, N 2. – P. 232.
10. Ehrburger P., Thrower P.A. Second international conference on carbon black // Carbon. – 1994. – V. 32, N 7. – P. 1303–1309.
11. Jones L.E., Thrower P.A., Walker P.L.Jr. Reactivity and related microstructure of 3d carbon/carbon composites // Carbon. – 1986. – V. 24, N 1. – P. 51–59.
12. Marx D.R., Thrower P.A. An investigation of stress effects on graphite oxidation // Carbon. – 1983. – V. 21, N 4. – P. 451–459.
13. Rodríguez-Mirasol J., Thrower P.A., Radovic L.R. On the oxidation resistance of C/C composites obtained by liquid-phase impregnation/ carbonization of different carbon cloths // Carbon. – 1993. – V. 31, N 5. – P. 789–799.
14. Marsh H., Rodríguez-Reinoso F. Activated carbon. London: Elsevier, 2006. – 536 p.
15. Lastoskie C., Gubbins K.E., Quirke N. Pore size distribution analysis of microporous carbons: a density functional theory approach // J. Phys. Chem. – 1993. – V. 97, N 18. – P. 4786–4796.
16. Seaton N.A., Walton J.P.R.B., Quirke N. A new analysis method for the determination of the pore size distribution of porous carbons from nitrogen adsorption measurements // Carbon. – 1989. – V. 27, N 6. – P. 853–861.
17. Jagiello J., Olivier J.P. A simple two-dimensional NLDFT model of gas adsorption in finite carbon // J. Phys. Chem. C. – 2009. – V. 113, N 45. – P. 19382–19385.
18. Ravikovitch P.I., Haller G.L., Neimark A.V. Density functional theory model for calculating pore size distributions: Pore structure of nanoporous catalysts // Adv. Colloid Interface Sci. – 1998. – V. 76–77. – P. 203–226.
19. Ravikovitch P.I., Neimark A.V. Characterization of nanoporous materials from adsorption and desorption isotherms // Colloid Surface Physicochem. Eng. Aspect. – 2001. – V. 187–188. – P. 11–21.
20. Ravikovitch P.I., Neimark A.V. Density functional theory model of adsorption on amorphous and microporous silica materials // Langmuir. – 2006. – V. 22, N 26. – P. 11171–11179.
21. Gusev Yu, O'Brien J.A., Seaton N.A. A self-consistent method for characterization of activated carbons using supercritical adsorption and grand canonical Monte Carlo simulations // Langmuir. – 1997. – V. 13, N. 10. – P. 2815–2821.
22. Thomson K.T., Gubbins K.E. Modeling structural morphology of microporous carbons by reverse Monte Carlo // Langmuir. – 2000. – V. 16, N. 13. – P. 5761–5773.
23. Liu J-C., Monson P.A. Molecular modeling of adsorption in activated carbon: comparison of Monte Carlo simulations with experiment // Adsorption. – 2005. – V. 11, N 1. – P. 5–13.
24. Palmer J.C., Brennan J.K., Hurley M.M., Balboa A., Gubbins K.E. Detailed structural models for activated carbons from molecular simulation // Carbon. – 2009. – V. 47, N 12. – P. 2904–2913.
25. Nguyen T.X., Cohaut N., Bae J-S., Bhatia S.K. New method for atomistic modeling of the microstructure of activated carbons using hybrid reverse Monte Carlo simulation // Langmuir. – 2008. – V. 24, N 15. – P. 7912–7922.
26. Quantachrome software, <http://www.quantachrome.com>.
27. Harris P.J.F. Fullerene-related structure of commercial glassy carbons // Philosoph. Mag. – 2004. – V. 84, N 29. – P. 3159–3167.
28. Harris P.J.F., Liu Z., Suenaga K. Imaging the atomic structure of activated carbon. // J. Phys: Condens Matter. – 2008. – V.20. – P. 362201–362205.
29. Terzyk A.P., Furmaniak S., Harris P.J.F. et al. How realistic is the pore size distribution calculated from adsorption isotherms if activated carbon is composed of fullerene-like fragments // Phys. Chem. Chem. Phys. – 2007. – V. 9. – P. 919–927.
30. Yang J-H., Cheng S-H., Wang X. et al. Quantitative analysis of microstructure of carbon materials by HRTEM // Trans. Nonferrous Met. Soc. China. – 2006. – V. 16. – P. 796–803.
31. Endos M., Furuta T., Minoura F. et al. Visualized observation of pores in activated carbon fibers by HRTEM and combined image

- processor // Supramol. Sci. – 1998. – V. 5. – P. 261–266.
32. Huang Z.-H., Kang F., Huang W.L. et al Pore structure and fractal characteristics of activated carbon fibers characterized by using HRTEM // J. Colloid Interface Sci. – 2002. – V. 249, N 2. – P. 453–457.
33. Palijczuk D., Gun'ko V.M., Leboda R. et al Porous structure of activated carbons and tert-butylbenzene breakthrough dynamics // J. Colloid Interface Sci. – 2002. – V. 250. – P. 5–17.
34. Gun'ko V.M., Turov V.V., Skubiszewska-Zięba J. et al. Structural characteristics of a carbon adsorbent and influence of organic solvents on interfacial water // Appl. Surf. Sci. – 2003. – V. 214. – P. 178–189.
35. Tomaszewski W., Gun'ko V.M., Leboda R., Skubiszewska-Zięba J. Interaction of amphetamines with micro- and mesoporous adsorbents in polar liquids // J. Colloid Interface Sci. – 2005. – V. 282. – P. 261–269.
36. Gun'ko V.M., Turov V.V., Leboda R. et al. Influence of organics on structure of water adsorbed on activated carbons // Adsorption. – 2005. – V. 11. – P. 163–168.
37. Gun'ko V.M., Palijczuk D., Leboda R. et al. Influence of pore structure and pretreatments of activated carbons and water effects on breakthrough dynamics of tert-butylbenzene // J. Colloid Interface Sci. – 2006. – V. 294. – P. 53–68.
38. Tomaszewski W., Gun'ko V.M., Leboda R., Skubiszewska-Zięba J. Interaction of methoxy- and methylenedioxymphetamines with carbon and polymeric adsorbents in polar liquids // Cent. Eur. J. Chem. – 2010. – V. 8. – P. 750–757.
39. Turov V.V., Gun'ko V.M., Leboda R. et al. Influence of organics on structure of water adsorbed on activated carbons // J. Colloid Interface Sci. – 2002. – V. 253. – P. 23–34.
40. Melillo M., Gun'ko V.M., Mikhalovska L.I. et al. Ibuprofen adsorption affected by bovine serum albumin // Langmuir. – 2004. – V. 20. – P. 2837–2851.
41. Mikhalovsky S.V., Gun'ko V.M., Turov V.V. et al. Investigation of structural and adsorptive characteristics of various carbons // Adsorption. – 2005. – V. 11. – P. 657–662.
42. Gun'ko V.M., Kozynchenko O.P., Turov V.V. et al. Structural and adsorption characteristics of activated carbons possessing significant textural porosity // Colloids Surf. A. – 2008. – V. 317. – P. 377–387.
43. Gun'ko V.M., Turov V.V., Kozynchenko O.P. et al. Characteristics of adsorption phase with water/organic mixtures at a surface of activated carbons possessing intraparticle and textural porosities // Appl. Surf. Sci. – 2008. – V. 254. – P. 3220–3231.
44. Gun'ko V.M., Turov V.V., Kozynchenko O.P. et al. Activation and structural and adsorption features of activated carbons with highly developed micro-, meso- and macroporosity // Adsorption. – 2011. – V. 17. – P. 453–460.
45. Gun'ko V.M., Meikle S.T., Kozynchenko O.P. et al. Comparative characterisation of carbon and polymer adsorbents by SAXS and nitrogen adsorption methods // J. Phys. Chem. C. – 2011. – V. 115. – P. 10727–10735.
46. Gun'ko V.M. Consideration of the multicomponent nature of adsorbents during analysis of their structural and energy parameters // Theoret. Experim. Chem. – 2000. – V. 36, N 1. – P. 319–324.
47. Gun'ko V.M., Do D.D. Characterization of pore structure of carbon adsorbents using regularization procedure // Colloids Surf. Physicochem. Eng. Aspect. – 2001. – V. 193, N 1–3. – P. 71–83.
48. Do D.D., Nguyen C., Do H.D. Characterization of micromesoporous carbon media // Colloids Surf. Physicochem. Eng. Aspect. – 2001. – V. 187–188. – P. 51–71.
49. Gun'ko V.M., Mikhalovsky S.V. Evaluation of slitlike porosity of carbon adsorbents // Carbon. – 2004. – V. 42, N 4. – P. 843–849.
50. http://pacific.mpi-cbg.de/wiki/index.php/Main_Page.
51. Image J. <http://rsbweb.nih.gov/ij/download.html>, accessed July 2007. Prodanov D. <http://rsb.info.nih.gov/ij/plugins/granulometry.html>, accessed August 2007.
52. Gun'ko V.M., Kozynchenko O.P., Tennison S.R. et al. Comparative study of nanopores in activated carbons by HRTEM and adsorption methods // Carbon. – 2012. – V. 50, Issue 9. – P. 3146–3153.
doi:10.1016/j.carbon.2011.10.009.
53. Landry M.R. Thermoporometry by differential scanning calorimetry: experimental considerations and applications // Thermochim. Acta. – 2005. – V. 433. – P. 27–50.
54. Weber J., Bergström L. Mesoporous hydrogels: revealing reversible porosity by cryoporometry, X-ray scattering, and gas adsorption // Langmuir. – 2010. – V. 26. – P. 10158–10164.
55. Brennan J.K., Bandosz T.J., Thomson K.T., Gubbins K.E. Water in porous carbon // Colloids Surf. A: Physicochemical and Engineering Aspects. – 2001. – V. 187–188. – P. 539–568.

Received 15.11.2011, accepted 26.03.2012

Порівняльний аналіз пористої структури та адсорбційних властивостей активованого вугілля

**В.М. Гунько, R. Leboda, J. Skubiszewska-Zięba, В.І. Зарко,
О.В. Гончарук, B. Charmas, С.В. Михаловський**

*Інститут хімії поверхні ім. О.О. Чуйка Національної академії наук України
вул. Генерала Наумова, 17, Київ, 03164, Україна, vlad_gunko@ukr.net
Університет імені Марії Кюрі-Склодовської, хімічний факультет
пл. Марії Кюрі-Склодовської, 3, Люблін, 20031, Польща
Університет Брайтона, Школа фармації та біомолекулярних наук
Брайтон, BN2 4GJ, Велика Британія*

Аналіз пористої структури різного активованого вугілля, виготовленого з натуральної сировини і полімерів, проводився з використанням СЕМ, АСМ, ПЕМ, адсорбції, ДСК і ТГ / ДТА методів. Незважаючи на велику пористість і високу питому поверхню, активоване вугілля погано адсорбує воду з повітря. Хоча велика кількість води заповнює значну (але не всю) частину пор при змочуванні водою, теплота змочування у воді значно менша ніж у декані. Розподіл пор за розміром, розрахований за адсорбцією і ДСК даними, узгоджується з результатами на основі аналізу HRTEM зображенів.

Сравнительный анализ пористой структуры и адсорбционных свойств активированного угля

**В.М. Гунько, R. Leboda, J. Skubiszewska-Zięba, В.И. Зарко,
Е.В. Гончарук, B. Charmas, С.В. Михаловский**

*Институт химии поверхности им. А.А. Чуйко Национальной академии наук Украины
ул. Генерала Наумова, 17, Киев, 03164, Украина, vlad_gunko@ukr.net
Университет имени Марии Кюри-Склодовской, химический факультет
пл. Марии Кюри-Склодовской, 3, Люблин, 20031, Польша
Университет Брайтона, Школа фармации и биомолекулярных наук
Брайтон, BN2 4GJ, Великобритания*

Анализ пористой структуры разных активированных углей, изготовленных из натурального сырья и полимеров, проводился с использованием СЭМ, АСМ, ПЭМ, адсорбции, ДСК и ТГ / ДТА методов. Несмотря на большую пористость и высокую удельную поверхность, активированные угли плохо адсорбируют воду из воздуха. Хотя большое количество воды заполняет значительную (но не всю) часть пор при смачивании водой, теплота смачивания в воде оказывается значительно меньше, чем в декане. Распределения пор по размерам, рассчитанные по адсорбции и ДСК данным, согласуются с результатами на основе анализа HRTEM изображений.